

# Half-Metallic Graphene Nanoribbons

Young-Woo Son,<sup>1,2</sup> Marvin L. Cohen,<sup>1,2</sup> and Steven G. Louie<sup>1,2</sup>

<sup>1</sup>Department of Physics, University of California at Berkeley, Berkeley, California 94720, USA

<sup>2</sup>Materials Sciences Division, Lawrence Berkeley National Laboratory, Berkeley, California 94720, USA

(Dated: submitted, March 25, 2006)

Electrical current can be completely spin polarized in a class of materials known as half-metals, as a result of the coexistence of metallic nature for electrons with one spin orientation and insulating for electrons with the other. Such asymmetric electronic states for the different spins have been predicted for some ferromagnetic metals—for example, the Heusler compounds<sup>1</sup>—and were first observed in a manganese perovskite<sup>2</sup>. In view of the potential for use of this property in realizing spin-based electronics, substantial efforts have been made to search for half-metallic materials<sup>3,4</sup>. However, organic materials have hardly been investigated in this context even though carbon-based nanostructures hold significant promise for future electronic device<sup>5</sup>. Here we predict half-metallicity in nanometre-scale graphene ribbons by using first-principles calculations. We show that this phenomenon is realizable if in-plane homogeneous electric fields are applied across the zigzag-shaped edges of the graphene nanoribbons, and that their magnetic property can be controlled by the external electric fields. The results are not only of scientific interests in the interplay between electric fields and electronic spin degree of freedom in solids<sup>6,7</sup> but may also open a new path to explore spintronics<sup>3</sup> at nanometre scale, based on graphene<sup>8,9,10,11</sup>

When a single graphite layer is terminated by zigzag edges on both sides, which we refer here to as a zigzag graphene nanoribbon (ZGNR) (Fig. 1), there are peculiar localized electronic states at each edge<sup>12,13</sup>. These edge states (which are extended along the edge direction) decay exponentially into the center of the ribbon, with decay rates depending on their momentum<sup>12,13,14,15</sup>. Such states have been observed in monoatomic step edges of graphite by using scanning probe techniques<sup>16,17</sup>. The localized edge states form a two-fold degenerate flat band at the Fermi energy ( $E_F$ ), existing in about one third of the Brillouin zone away from the zone center<sup>12,13,14,15</sup>. By invoking band ferromagnetism, it has been suggested that an opposite spin orientation across the ribbon between ferromagnetically ordered localized edge states on each edge in ZGNRs is the ground-state spin configuration; that is, the total spin is zero<sup>12,18,19</sup>. Because the states around  $E_F$  are the edge states and linear combinations of them, the effects of external transverse fields are expected to be significant on these states, in contrast with those on the extended states<sup>20</sup>.

Our study of the spin resolved electronic structure of

ZGNRs is based on the *ab initio* pseudopotential density functional method<sup>21</sup> within the local spin density approximation<sup>22</sup>. A periodic saw-tooth-type potential perpendicular to the direction of the ribbon edge is used to simulate the external electric fields ( $E_{\text{ext}}$ ) in a supercell (Fig. 1). In accordance with previous convention<sup>12,13,14,15</sup>, the ZGNRs are classified by the number of zigzag chains ( $n$ ; Fig. 1) forming the width of the ribbon. We will hereafter refer to an ZGNR with  $n$  zigzag chains an  $n$ -ZGNR. When the spin degree of freedom is neglected, our calculation from first-principles also predicts a two-fold degenerate flat band at  $E_F$  (Fig. 2a). But the spinless state is not the ground state. Moreover, the electronic structures of the ZGNRs show marked alterations when spins and  $E_{\text{ext}}$  are included.

Considering first the spin degree of freedom, we find as in previous studies that the configuration with opposite spin (antiferromagnetic) orientation between ferromagnetically ordered edge states at each edge (Fig. 2b) is favored as the ground state over the configuration with same spin orientation between the two edges<sup>12,18,19</sup>. (The present result of antiferromagnetic spin configuration on the honeycomb lattice is consistent with a theorem for electrons on bipartite lattice<sup>23</sup>.) Our calculations show that the magnetic interaction energies are quite large.

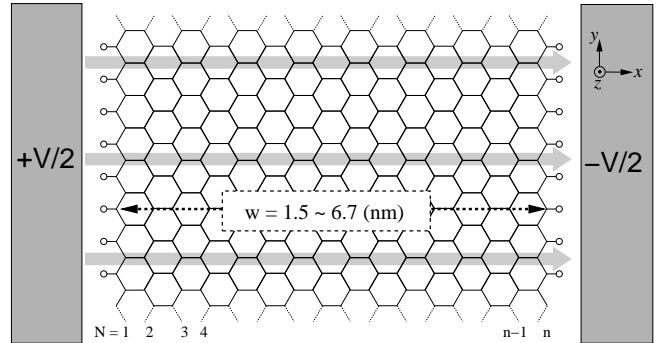


FIG. 1: **Graphene nanoribbon in electric fields.** Diagram of a zigzag graphene nanoribbon (ZGNR) with external transverse electric field  $E_{\text{ext}}$ .  $E_{\text{ext}}$  is applied across the ZGNR along the lateral direction ( $x$  direction) in an open circuit split-gate configuration and is positive towards the right side. The ZGNRs are assumed to be infinite along the  $y$  direction. A small longitudinal source-drain field could be applied to generate spin-polarized currents along the  $y$ -direction. Hydrogen atoms on the edges are denoted by circles. The ZGNR shown in this figure is an 16-ZGNR ( $n=16$ ). The width  $w$  of ZGNRs under study was in the range  $1.5 \sim 6.7$  nm.

For example, the total energy difference between a spin-polarized edge and a spin-unpolarized one is 20 meV per edge atoms in the case of 8-ZGNR, and the spin configuration is further stabilized by 2.0 meV per edge atom due to the antiferromagnetic coupling between the spin-polarized edges. Because the interaction between spins on opposite edges increases with decreasing width, the total energy of an  $n$ -ZGNR with antiferromagnetic arrangement across opposite edges is always lower than that of a ferromagnetic arrangement if  $n \leq 32$ . This total energy hierarchy is maintained when external electric fields are applied. It is known that spontaneous magnetic orderings in one- and two-dimensional spin lattice model are difficult to achieve at finite temperature<sup>24</sup>. Spin correlation lengths comparable to nanoscale systems, however, is possible in practice<sup>25,26,27,28</sup>. Here, we also expect that spin orderings are realizable because of the large anisotropic exchange interactions between the spins in ribbons with split-gate geometry on the substrate.

We find that the ground state of the ZGNRs, including spin degree of freedom, has a bandgap which is inversely proportional to the ribbon width. However, the energy splitting at  $ka = \pi$  is  $\sim 0.52$  eV regardless of width if  $n \geq 8$ . The states of opposite spin orientation are degenerate in all bands (Fig. 2c, left). When spins are included, the degeneracy between the occupied and unoccupied edge-

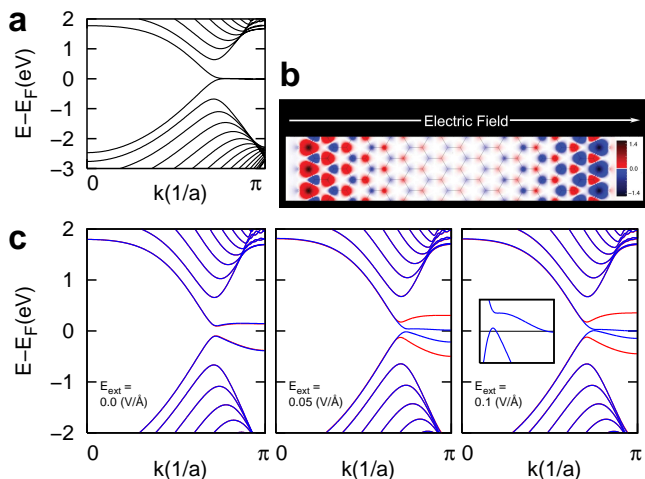


FIG. 2: **Electronic structures of graphene nanoribbons.** In all the figures, the Fermi energy ( $E_F$ ) is set to zero. **a**, The spin-unpolarized band structure of an 16-ZGNR. **b**, The spatial distribution of the charge difference between  $\alpha$ - and  $\beta$ -spin ( $\rho_\alpha(r) - \rho_\beta(r)$ ) for the ground state when there is no external field. The magnetization per edge atom for each spin on each sublattice is  $0.43 \mu_B$  with opposite orientation, where  $\mu_B$  is the Bohr magneton. The graph is the density integrated in  $z$  direction and the scale bar is in unit of  $10^{-2} |e|/\text{\AA}^2$ . **c**, From left to right, the spin-resolved band structures of an 16-ZGNR with  $E_{\text{ext}} = 0.0, 0.05,$  and  $0.1$  V/\AA, respectively. The red and blue lines denote bands of  $\alpha$ -spin and  $\beta$ -spin states, respectively. Inset, the band structure with  $E_{\text{ext}} = 0.1$  V/\AA in the range  $|E - E_F| < 50$  meV and  $0.7\pi \leq ka \leq \pi$  (the horizontal line is  $E_F$ ).

state bands at  $E_F$  is now lifted and the edge states near  $E_F$  have dispersion along the direction of the edge with a band width of  $\sim 2$  eV when extended over the Brillouin zone.

With applied transverse electric fields, we find that the valence and conduction edge-state bands associated with one spin orientation close their gap, whereas those associated with the other widen theirs (Fig. 2c). So, under appropriate field strengths, the ZGNRs are forced into a half-metallic state by the applied electric field, resulting in insulating behavior for one spin and metallic behavior for the other. We shall defer the discussion of spin-orbit interactions later. For now, we label the gap-opening states as  $\alpha$ -spin (shown in red in Figs 2-4) and the gap-narrowing states as  $\beta$ -spin (blue). In a 16-ZGNR, the bandgap associated with  $\beta$ -spin is completely closed by an  $E_{\text{ext}} = 0.1$  V/\AA, whereas the gap for  $\alpha$ -spin electrons remains very large at 0.30 eV (Fig. 2c). The energy gap for the  $\beta$ -spin electrons changes to an indirect gap from a direct gap as  $E_{\text{ext}}$  increased, and is closed indirectly (Fig. 2c, inset). After gap closure, an electron channel near  $ka = \pi$  and a hole channel near  $ka = 0.75\pi$  appear at  $E_F$ , all with the same spin direction.

The half-metallicity of the ZGNRs originates from the fact that the applied electric fields induce energy level shifts of opposite signs for the spatially separated spin ordered edge states. Such separate and opposite energy shifts are made possible by the localized nature of the edge states around  $E_F$ . Because oppositely oriented spin states are located at the opposite sides of the ZGNR, the effect of  $E_{\text{ext}}$  on them is opposite, moving the occupied and unoccupied  $\beta$ -spin states closer in energy but moving the occupied and unoccupied  $\alpha$ -spin states apart (Fig. 3). The electrostatic potential is raised on the right side and lowered on the left side as  $E_{\text{ext}} (> 0)$  increases. Correspondingly, the energies for localized edge states on the right side are shifted upward and those on the left side downwards, eventually leaving states of only one spin orientation at  $E_F$  (Fig. 3b). In a 16-ZGNR, the occupied  $\alpha$ -spin states and unoccupied  $\beta$ -spin states on the left side move downwards in energy by 19 meV and 110 meV, respectively, and occupied  $\beta$ -spin and unoccupied  $\alpha$ -spin states on the right side upwards by 112 meV and 74 meV, respectively, as  $E_{\text{ext}}$  increases to 0.1 V/\AA (Fig. 3c). The occupied  $\beta$ -spin states in the middle of a 16-ZGNR are the tails of the localized  $\beta$ -spin states on the right side and the unoccupied  $\beta$ -spin states are from the left side, so that occupied and unoccupied  $\beta$ -spin states in the middle of the ZGNR move oppositely to close the gap. The energies of the occupied and unoccupied  $\alpha$ -spin states in the middle also follow movements of those of the corresponding localized states on each side, resulting in an increased gap value (Fig. 3c).

We note that the critical electric field for achieving half-metallicity in ZGNRs decreases as the width increases because the electrostatic potential difference between the two edges is proportional to the system size. For a 32-ZGNR whose width is  $67.2\text{\AA}$ ,  $E_{\text{ext}} = 0.045$

$V/\text{\AA}$  is required to close the band gap for the  $\beta$ -spin electrons (Fig. 4). Because the energy shifts of the edge states depends on the total voltage drop between the two sides, the variation of the energy gap is expected to exhibit a universal behavior as function of  $wE_{\text{ext}}$  where  $w$  is the width of the ZGNR. This is seen in the inset in Fig. 4. From the calculations, the required critical field is estimated to be  $3.0 (V)/w(\text{\AA})$ . To establish half-metallicity, the relevant energy scale is given by the field-induced en-

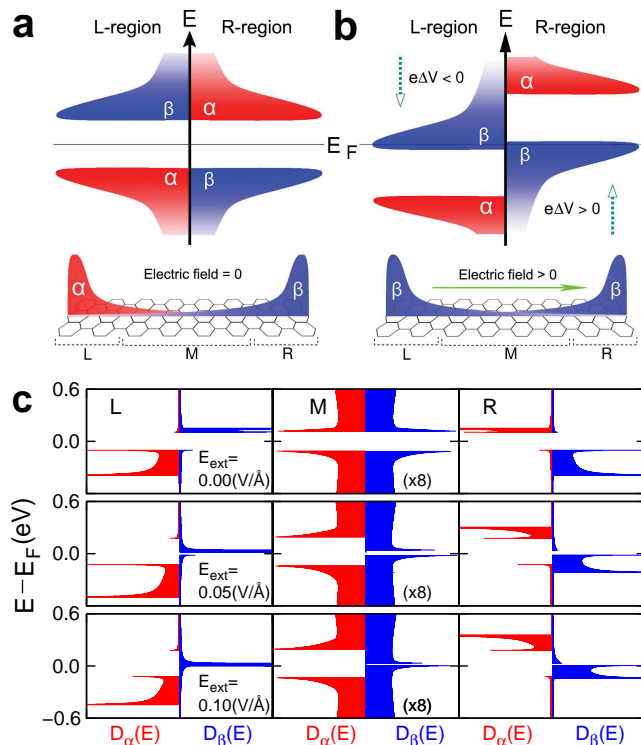


**FIG. 3: Origin of half-metallicity.** **a**, Schematic density of states diagram of the electronic states of a ZGNR in the absence of an applied electric field. Top: the occupied and unoccupied localized edge states on left side (L-region as defined at the bottom) are  $\alpha$ -spin and  $\beta$ -spin states, respectively, and vice versa on right side (R-region) with the same energy gap for both sides. Bottom: schematic diagram of the spatial spin distribution of the highest occupied valence band states without an external electric field. **b**, Top: with a transverse electric field, the electrostatic potential on the left side is lowered ( $e\Delta V < 0$ ) while the one on the right side is raised ( $e\Delta V > 0$ ). Correspondingly, the energies of the localized state at the left edge are decreased and those of the localized states at right edge increased. Bottom: the resulting states at  $E_F$  are only  $\beta$ -spin. **c**, From left to right, the local density of states of  $\alpha$ - and  $\beta$ -spins (ordinate) of a 16-ZGNR as a function of energy (abscissa) for atoms in the L, M and R regions shown in **a**, respectively. From top to bottom,  $E_{\text{ext}} = 0.0, 0.05$  and  $0.1 \text{ V/\AA}$  respectively. The local density of states in the middle panels are enlarged eightfold for clarity. For  $E_{\text{ext}} = 0.1 \text{ V/\AA}$ , the van Hove singularities of  $\beta$ -spin in the M and R region are above the  $E_F$  by 5 meV, and all states at  $E_F$  are of  $\beta$ -spin.

ergy shift, and its magnitude is in the order of 100 meV. Thus the small magnitude of spin-orbit interaction (4~6 meV) in carbon atoms<sup>29,30</sup> would not change the half-metallic nature of the ZGNRs, but would function in determining the spatial direction (normal direction with respect to the ribbon plane) of spin up and down in the ZGNRs<sup>29</sup>.

Because edges are inevitably susceptible to defects, we have examined the robustness of the predicted half-metallicity to edge defects. Our calculations show that the system remains purely of one spin-type at  $E_F$  in the presence of different type and concentration of defects. Results on 8-ZGNRs with three different kinds of defects (dangling bonds, vacancies, and Stone-Wales defects at 6~12% defect concentration per edge) are presented in Supplementary Fig. 1, confirming that the predicted half-metallicity is indeed robust.

Another consideration is that, when in the half-metallic state the ZGNRs are in a transverse electric field, the current-carrying electrons moving from the source to the drain in the longitudinal direction would experience an effective magnetic field due to spin-orbit interactions<sup>6,7</sup> and the spins are expected to rotate. However, we find that the resulting extremely weak effective magnetic field are parallel to the spatial spin direction ( $z$ -direction in Fig. 1) already determined by the intrinsic spin-orbit interaction of carbon atoms. Supposed that we have  $\beta$ -spin electrons moving with velocity  $\vec{v} = v\hat{y}$  in  $\vec{E} = E_{\text{ext}}\hat{x}$ , the effective magnetic field exerted on the

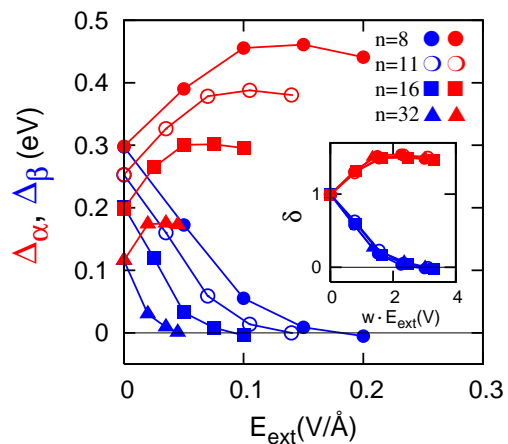


**FIG. 4: Dependence of half-metallicity on system size.**  $\Delta_\alpha$  (red) denotes the direct band gap of  $\alpha$ -spin, and  $\Delta_\beta$  (blue) the (in)direct gap of  $\beta$ -spin as function of  $E_{\text{ext}}$  for 8-ZGNR (filled circles), 11-ZGNR (open circles), 16-ZGNR (squares), and 32-ZGNR (triangles). The slope variation of  $\Delta_\alpha$  and  $\Delta_\beta$  indicates gap change from direct to indirect. The rescaled gap  $\delta_\alpha(w, E_{\text{ext}}) \equiv \Delta_\alpha(w, E_{\text{ext}})/\Delta_0(w)$  and  $\delta_\beta(w, E_{\text{ext}}) \equiv \Delta_\beta(w, E_{\text{ext}})/\Delta_0(w)$  for the various widths collapse to a single function of  $wE_{\text{ext}}$  as shown in the inset, where  $\Delta_\alpha(w, E_{\text{ext}})$  and  $\Delta_\beta(w, E_{\text{ext}})$  are the bandgap for  $\alpha$ -spins and  $\beta$ -spins, respectively, of the ZGNR with a width of  $w$  in  $E_{\text{ext}} (\neq 0)$ , and  $\Delta_0(w) \equiv \Delta_\alpha(w, E_{\text{ext}} = 0) = \Delta_\beta(w, E_{\text{ext}} = 0)$ .

$\beta$ -spin electrons would be  $\vec{B}_{\text{eff}} = \frac{ev\hbar}{4mc^2} E_{\text{ext}} \hat{z}$  where  $\hbar$  is the Planck constant,  $m$  is the mass of an electron,  $e$  is the charge on an electron, and  $c$  is the speed of light. At a critical electric field of  $0.045 \text{ V/\AA}$  for a 32-ZGNR, the estimated energy for spin-orbit coupling due to  $E_{\text{ext}}$  is only  $1.1 \times 10^{-4} \text{ meV}$ . We also find that, as a result of the energy gap asymmetry for each spin, there is no spin precession even when the direction of  $E_{\text{ext}}$  is tilted or when the spatial spin direction is altered by spin-orbit interaction arising from the substrate. So, the spatial spin direc-

tion once determined would not change even if a strong transverse electric field is applied. This implies that, if we change the direction of  $E_{\text{ext}}$ , the spin-polarity of the carriers at  $E_F$  of the half-metallic ribbon will be reversed because the induced potentials at the edges change their signs. Hence, under these conditions, the half-metallic nature is robust even though a transverse electric fields is applied, and spin polarized current should be obtained in transport experiment with split-gates.

- 
- <sup>1</sup> de Groot, R. A., Mueller, F. M., van Engen, P. G. & Buschow, K. H. J. New class of materials: half-metallic ferromagnets. *Phys. Rev. Lett.* **50**, 2024–2027 (1983).
- <sup>2</sup> Park, J.-H. *et al.* Direct evidence for a half-metallic ferromagnet. *Nature* **392**, 794–796 (1998).
- <sup>3</sup> Wolf, S. A. *et al.* Spintronics: A spin-based electronics vision for the future. *Science* **294**, 1488–1495 (2001).
- <sup>4</sup> Fang, C. M., de Wijs, G. A. & de Groot, R. A. Spin-polarization in half-metals, *J. Appl. Phys.* **91**, 8340–8344 (2002).
- <sup>5</sup> McEuen, P. L., Fuhrer, M. S. & Park, H. Single-walled carbon nanotube electronics, *IEEE Trans. Nanotechnol.* **1**, 78–85 (2002).
- <sup>6</sup> Murakami, S., Nagaosa, N. & Zhang, S.-C. Dissipationless quantum spin current at room temperature. *Science* **301**, 1348–1351 (2003).
- <sup>7</sup> Sinova, J. *et al.* Universal intrinsic spin Hall effect. *Phys. Rev. Lett.* **92**, 126603 (2004).
- <sup>8</sup> Berger, C. *et al.* Ultrathin epitaxial graphite: 2D electron gas properties and a route toward graphene-based nanoelectronics. *J. Phys. Chem. B* **108**, 19912–19916 (2004).
- <sup>9</sup> Novoselov, K. S. *et al.* Two-dimensional gas of massless Dirac fermions in graphene. *Nature* **438**, 197–200 (2005).
- <sup>10</sup> Zhang, Y., Tan, Y.-W., Stormer, H. L. & Kim, P. Experimental observation of the quantum Hall effect and Berry’s phase in graphene. *Nature* **438**, 201–204 (2005).
- <sup>11</sup> Berger, C. *et al.* Electronic confinement and coherence in patterned epitaxial graphene. *Science* **312**, 1191–1196 (2006).
- <sup>12</sup> Fujita, M., Wakabayashi, K., Nakada, K., & Kusakabe, K. Peculiar localized state at zigzag graphite edge. *J. Phys. Soc. Jpn.* **65**, 1920–1923 (1996).
- <sup>13</sup> Nakada, K., Fujita, M., Dresselhaus, G. & Dresselhaus, M. S. Edge state in graphene ribbons: nanometer size effect and edge shape dependence. *Phys. Rev. B* **54**, 17954–17961 (1996).
- <sup>14</sup> Wakabayashi, K., Fujita, M., Ajiki, H. & Sgrist, M. Electronic and magnetic properties of nanographite ribbons. *Phys. Rev. B* **59**, 8271–8282 (1999).
- <sup>15</sup> Miyamoto, Y., Nakada, K. & Fujita, M. First-principles study of edge states of H-terminated graphitic ribbons. *Phys. Rev. B* **59**, 9858–9861 (1999).
- <sup>16</sup> Kobayashi, Y., Fukui, K.-I., Enoki, T., Kusakabe, K. & Kaburagi, Y. Observation of zigzag and armchair edges of graphite using scanning tunneling microscopy and spectroscopy. *Phys. Rev. B* **71**, 193406 (2005).
- <sup>17</sup> Niimi, Y. *et al.* Scanning tunneling microscopy and spectroscopy of the electronic local density of states of graphite surfaces near monoatomic step edges. *Phys. Rev. B* **73**, 085421 (2006).
- <sup>18</sup> Okada, S. & Oshiyama, A. Magnetic ordering in hexagonally bonded sheets with first-row elements. *Phys. Rev. Lett.* **87**, 146803 (2001).
- <sup>19</sup> Lee, H., Son, Y.-W., Park, N., Han, S. & Yu, J. Magnetic ordering at the edges of graphitic fragments: Magnetic tail interactions between the edge-localized states. *Phys. Rev. B* **72**, 174431 (2005).
- <sup>20</sup> Son, Y.-W., Ihm, J., Cohen, M. L., Louie, S. G. & Choi, H. J. Electrical switching in metallic carbon nanotubes. *Phys. Rev. Lett.* **95**, 216602 (2005).
- <sup>21</sup> Soler, J. M. *et al.* The SIESTA method for *ab initio* order-N materials simulation. *J. Phys. Condens. Matter* **14**, 2745–2779 (2002).
- <sup>22</sup> Perdew, J. P. & Zunger, A. Self-interaction correction to density-functional approximations for many-electron systems. *Phys. Rev. B* **23**, 5048–5079 (1981).
- <sup>23</sup> Lieb, E. H. Two theorems on the Hubbard model. *Phys. Rev. Lett.* **62**, 1201–1204 (1989).
- <sup>24</sup> Mermin, N. D. & Wagner, H. Absence of ferromagnetism or antiferromagnetism in one- or two-dimensional isotropic Heisenberg models. *Phys. Rev. Lett.* **17**, 1133–1136 (1966).
- <sup>25</sup> Gambardella, P. *et al.* Ferromagnetism in one-dimensional monatomic metal chains. *Nature* **416**, 301–304 (2002).
- <sup>26</sup> Dorantes-Dávila, J. & Pastor, G. M. Magnetic anisotropy of one-dimensional nanostructures of transition metals. *Phys. Rev. Lett.* **81**, 208–211 (1998).
- <sup>27</sup> Vindigi, A., Rettori, A., Pini, M. G., Carbone, C. & Gambardella, P. Finite-sized Heisenberg chains and magnetism of one-dimensional metal systems, *Appl. Phys. A* **82**, 385–394 (2006).
- <sup>28</sup> Delin, A., Tossati, E. & Weht, R. Magnetism in atomic-size palladium contacts and nanowires. *Phys. Rev. Lett.* **92**, 057201 (2004).
- <sup>29</sup> Yao, Y., Ye, F., Qi, X.-L., Zhang, S.-C., & Fang, Z. Spin-orbit gap of graphene. Preprint at <http://arxiv.org/abs/cond-mat/0606350> (2006).
- <sup>30</sup> Min, H. *et al.* Intrinsic and Rashba spin-orbit interactions in graphene sheets. Preprint at <http://arxiv.org/abs/cond-mat/0606504> (2006).

**Acknowledgements** We thank J. Neaton, F. Giustino, I. Souza, C. H. Park and H. J. Choi for discussions. This research was supported by National Science Foundation (NSF) and by the Director, Office of Science, Office of Basic Energy Science, Division of Material

Sciences and Engineering, U.S. Department of Energy (DOE). Computational resources have been provided by the NSF at the National Partnership for Advanced Computational Infrastructure and by the DOE at the National Energy Research Scientific Computing Center.

**Author Information** The authors declare no competing financial interests. Correspondence and requests for materials should be addressed to S.G.L. (e-mail: sglouie@berkeley.edu).

## Supplementary Figure and Legend

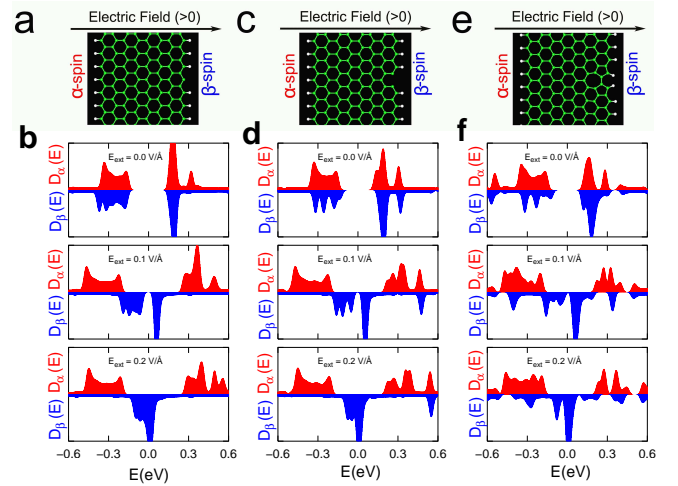


**FIG. 5: Supplementary Fig1. Robustness of half-metallicity in defective graphene nanoribbons.** **a**, A ball-and-stick model of an 8-ZGNR with one dangling bond (an edge carbon atom without hydrogen passivation) on the right edge. One dangling bond per 17 edge atoms are considered, which corresponds to 5.9% impurity concentration per one edge. In the figure, the atomic structure near the defect is displayed. Electric fields ( $E_{\text{ext}} > 0$ ) are applied from the left side to the right side. The  $\alpha$ -spin state is located on the left side and the  $\beta$ -spin state on the right side in the case of the ground state without applied electric fields. **b**, From top to bottom panels, the spin resolved total density of states (TDOS) are drawn for a defective 8-ZGNR shown in **a** with  $E_{\text{ext}} = 0.0, 0.1,$  and  $0.2 \text{ V/\AA}$  respectively. At the same critical  $E_{\text{ext}}$  of  $0.2 \text{ V/\AA}$  for an ideal 8-ZGNR, the gap for  $\beta$ -spin state is completely closed. **c**, A ball-and-stick model of an 8-ZGNR with one carbon-atom vacancy on the right edge. Defect concentration, ground spin configuration, and direction of electric fields are identical to the case of an 8-ZGNR with one dangling bond shown in **a**. **d**, The TDOS for an 8-ZGNR with one vacancy on the right edge (shown in **c**) with and without electric fields. Half-metallic nature persists also in this case. **e**, A ball-and-stick model for an 8-ZGNR with one single rotated bond (Stone-Wales defect at the right edge). Impurity concentration per one edge in this case is 11.8% since two edge atoms participate to create a Stone-Wales (SW) defect. Electric fields and ground spin configuration follow the same convention described in **a** and **c**. The total energy of an 8-ZGNR with a SW defect is much higher than that of the ideal one by 3.05 eV per defect so that appropriate treatments (e.g. annealing) on the sample will remove this highly unstable defect of this kind. Nevertheless, even with such high impurity concentration shown in **e**, the TDOSs displayed in **f** clearly show the robustness of the half-metallicity since the gap for the  $\beta$ -spin states is completely closed while the gap for  $\alpha$ -spin state is at 0.39 eV with  $E_{\text{ext}} = 0.2 \text{ V/\AA}$ .